Tribology Letters (2020) 68:30
https://doi.org/10.1007/s11249-019-1245-9

ORIGINAL PAPER

Effect of Environment on Microstructure Evolution and Friction of Au–Ni Multilayers

Ebru Cihan[1] · Katherine Jungjohann[2] · Nicolas Argibay[3] · Michael Chandross[3] · Martin Dienwiebel[1,4]

Received: 29 August 2019 / Accepted: 9 November 2019 / Published online: 29 January 2020

Abstract

We present results from a systematic investigation of environmental effects on the frictional behavior of Au–Ni multilayer films of varying interlayer spacing. The current results, sliding against ruby spheres in a dry N_2 atmosphere, are compared to prior work on the tribological behavior of these materials under ultra-high vacuum (UHV) (Cihan et al. in Sci Rep 9:1–10, 2019). Under both conditions, there is a regime of high friction when the interlayer spacing is large and a regime of low friction when the spacing is small. The low friction regime is associated with a critical grain size below which grain boundary sliding is expected to be the dominant mechanism of deformation. A shear-induced alloy formation (60–65 at.% Ni in Au) and a concomitant low friction coefficient was observed with multilayer spacings of 20 nm and lower under UHV. A distinct microstructure was found in dry N_2, and is attributed to different interfacial characteristics due to adsorbed species; rather than mixing between Au and Ni layers, only the uppermost Au layers were affected by shearing. These observations are coupled with the friction and wear behavior of multilayer samples sliding under different environments.

Keywords Multilayer · Au–Ni · Friction · Plasticity · Dislocation · Grain boundary · Nanocrystalline

1 Introduction

The environmental conditions under which tribological materials operate in industrial applications are generally not the same as those used during the process design. For example, special sliding components operated under ultra-high vacuum (UHV) conditions (i.e., in space technology or in lithography) must be designed to provide low friction under vacuum [1]. Moreover, fundamental friction studies and atomistic simulations are often performed in a vacuum environment in order to reduce the complexity of the observed phenomena and the computational effort, even though these are not the conditions under which the application may operate [2].

However, the environment can have a profound impact on the friction and wear of the contacting material surfaces, as adsorbed contaminants can cause changes at the asperity level and so-called third bodies [3] are generated with different chemical compositions and morphologies [4]. Therefore, it is important to understand the environmental effects on friction and wear of different metallic materials, and to that end, several experiments have been carried out at both the microscale [5–12] and nanoscale [13–16].

✉ Martin Dienwiebel
martin.dienwiebel@kit.edu

Ebru Cihan
ebru.cihan@ap.physik.uni-giessen.de

Katherine Jungjohann
kljungj@sandia.gov

Nicolas Argibay
nargiba@sandia.gov

Michael Chandross
mechand@sandia.gov

[1] Institute for Applied Materials-Computational Materials Science (IAM-CMS), Karlsruhe Institute of Technology (KIT), 76131 Karlsruhe, Germany

[2] Center for Integrated Nanotechnologies (CINT), Sandia National Laboratories, Albuquerque, NM 87185, USA

[3] Material, Physical, and Chemical Sciences Center, Sandia National Laboratories, Albuquerque, NM 87185, USA

[4] Fraunhofer Institute for Mechanics of Materials (IWM), MicroTribology Center µTC, 79108 Freiburg, Germany

At the microscale, the subsurface microstructure is affected by structural modifications due to the large plastic strain gradients generated during sliding of the surfaces in contact. These instabilities can lead to folding or cracking at the subsurface. An increase in the coefficient of friction (COF) is usually observed due to increased roughness at a sliding surface that is more easily plowed. Furthermore, wear debris particles may develop, and mechanical mixing/alloying between these particles and the sliding surface can create a nanostructured tribomaterial that lowers the COF. At higher sliding cycles the COF may increase [17] due to delamination of this tribomaterial.

The adsorption of molecules under ambient conditions can lead to film formation at the surface and mechanical mixing with the near surface volume. The most frequently encountered state here is the formation of oxide films that are usually between 1 and 10 nm thick [18]. In such cases, the sliding behavior is controlled by the structure of these oxide films. If the oxide film is penetrated or removed during sliding, then the COF transitions rapidly to a value that is determined by the interaction of the base materials [19]. However, if the oxide layer is not broken, the oxide accommodates the shear, and determines the friction force. In the presence of an oxide or another reaction-formed film at the interface, recorded COF values in air are often much lower than in vacuum. The higher friction under vacuum is often attributed to strong adhesion between contacting clean metal surfaces. Growth of junctions can also take place, depending on the ductility of the asperity material [20].

In this article, we present a systematic experimental study of the frictional behavior of Au–Ni multilayer samples, with different interlayer spacing, under a well-controlled N_2 atmosphere, and present a comprehensive comparison with our previous UHV results [21]. Because Au and Ni are immiscible under certain conditions (e.g. conditions provided during deposition of the layers in this study), they were chosen to analyze the effect of microstructure on friction [21]. We clarify what influence of the initial microstructure of these Au–Ni multilayer samples is observed in a dry N_2 environment.

2 Experimental Procedure

2.1 Preparation and Characterization of Au–Ni Multilayers

Ex situ cleaning of Si wafers (100) took place in two steps. A tenside surfactant was used as the pre-cleaner in an effort to achieve rough cleaning of the substrates, followed by an acetone solution in an ultrasonic bath for 2 h for the final stage. To clean and activate the substrate surface, plasma etching was applied inside a physical vapor deposition (PVD) chamber (Leybold Z550) for 2 min at an atmosphere of 0.5 Pa Ar in 6 N and a power of 500 W. Subsequently, the growth of Ni and Au layers with well-defined microstructures on Si substrates took place via magnetron sputtering at 0.4 Pa Ar in 6 N purity atmosphere with 75 mm diameter elemental targets. The individual layer thicknesses were 10 nm, 20 nm, 50 nm, or 100 nm, and the number of layers was changed from 100 to 10 to fix the total layer thickness at 1 µm. In order to prevent possible oxidation, in all cases the topmost layer was Au followed by Ni.

For the characterization of the friction-induced microstructure, multilayer samples were milled via focused ion beam (FIB) (FEI Helios Nanolab 650, now ThermoFisher, operated at 30 kV) following the procedure for in-situ lift out technique reported in [22]. The cross sections were prepared either parallel (longitudinal plane) or perpendicular (transverse plane) to the sliding direction. Figure 1 provides a survey of the cross-sectional view of the as-grown Au–Ni multilayer samples using high annular angle dark field (HAADF) mode thorough the scanning transmission electron microscope (STEM) detector. The waviness seen between the Au and Ni layers is due to residual strains, possibly induced by the lattice mismatch (~ 15%) between these metals, as well as orientation dependent growth rates. To analyze the worn microstructures and investigate their subsurface chemistry (S)TEM (FEI Titan ChemiSTEM, operated at 200 kV) imaging, operated in both the bright field (BF) and the HAADF mode, in combination with the energy dispersive X-ray spectroscopy (EDXS) analyses were performed on the multilayer samples. TEM and high resolution (HR) TEM (FEI Tecnai F30, operated at 300 kV) were also used.

In order to identify the crystallographic features of the multilayer samples, X-ray diffraction (XRD) analysis was performed. The measurements were carried out using $CuK\alpha_{1/2}$ radiation in Bragg–Brentano geometry at a Seifert PAD II diffractometer equipped with a Meteor 1D detector. The presence of Au (111) crystallographic planes and possible Ni (111) planes, which have similar diffraction angle with the (200) order of Au, was confirmed.

A commercial AFM (Veeco Dimension V, now Bruker) was used in contact mode to analyze the roughness of the uppermost layers of Au–Ni multilayer samples to study the effects of layer thickness on surface roughness. Si cantilevers (Budget Sensors uncoated Tap300 series with a radius of curvature < 10 nm, a resonant frequency of 300 kHz and a spring constant of 40 N/m) were used. It was observed that the roughness increases only slightly with layer thickness.

A Hysitron TI 950 Triboindenter (Bruker) nanoindenter was used to determine the hardness of the as-grown Au–Ni multilayer samples through indentation load–displacement curves. A Berkovich-type diamond triangular pyramidal indenter was used. It was observed that an increase in the

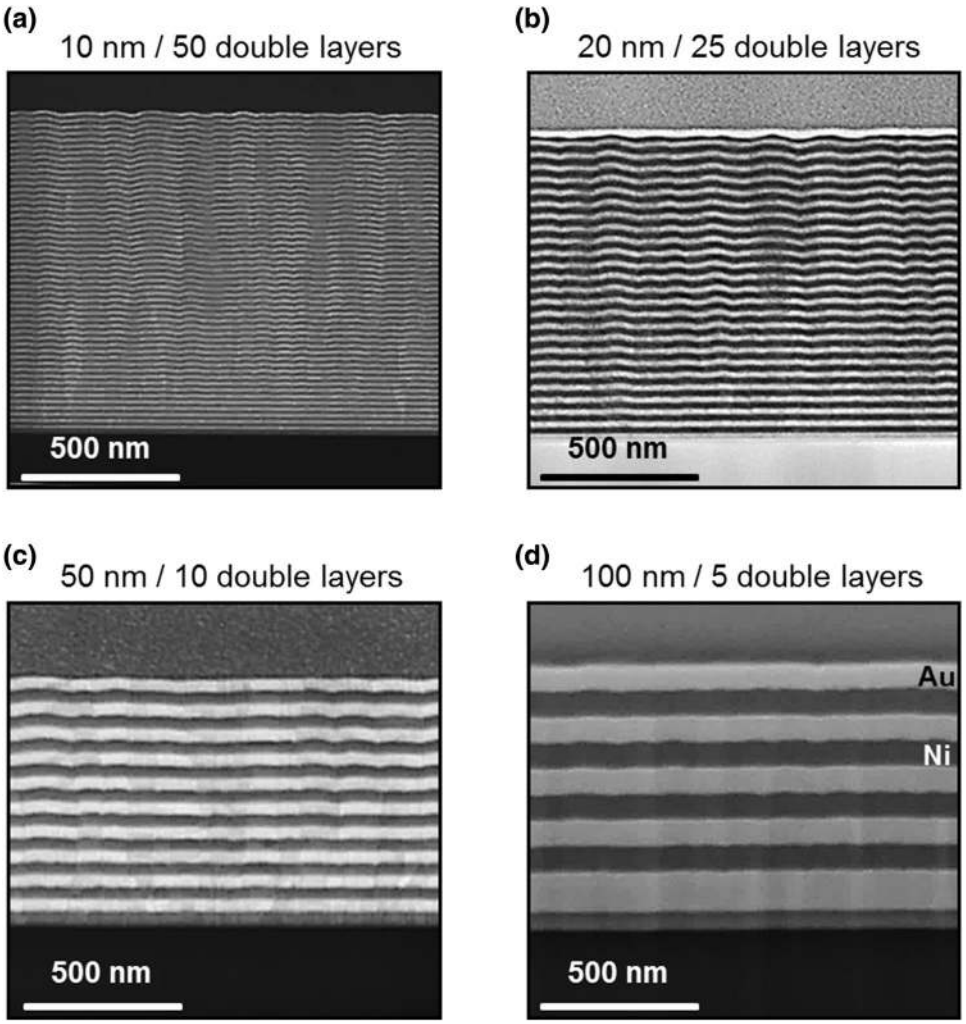

Fig. 1 HAADF STEM cross-sectional views of the as-grown Au–Ni multilayers for interlayer spacings of 10 nm (**a**), 20 nm (**b**), 50 nm (**c**) and 100 nm (**d**), respectively

layer thickness from 10 to 100 nm leads to decrease in hardness of the multilayers by 58.3% ± 7% at an 8 mN indentation load.

2.2 Microtribological Experiments

A microtribometer in a polymer glove box, purged with dry N_2 to < 10 ppm O_2 and < 40 ppm H_2O, was used for friction experiments at ambient temperature. The relative humidity varied in the range of 10–20% and the temperature was 20 ± 1 °C during testing. A 1 mN normal load was applied on an inert ruby sphere (3.2 mm in diameter) and slid against a flat silicon wafer coated with Au–Ni multilayers at 33 μm/s for 100 reciprocating cycles, using a stroke length of 1 mm. The tribometer consists of a two-axis double-leaf spring cantilever where friction and normal force are determined using capacitance probes that measure displacement of the calibrated cantilever (further details are found in [23]).

3 Results

3.1 Frictional Behavior

Figure 2a shows the friction coefficient as a function of cycle number. For all experiments, the friction coefficient drops after the first few cycles, and for some multilayer samples the COF decreases gradually (e.g., 10 nm layer spacing), while for others it decreases suddenly. The experiments on multilayer samples with 20 and 50 nm layer spacings still showed unstable behavior towards the end of the experiments, whereas for the other systems stable friction was observed within the last 20 cycles. As shown in Fig. 2b, c, the COF increases with increasing layer thickness at the last cycle (Fig. 2b) and when averaged over the last five cycles (Fig. 2c). In the remainder of the paper we will not discuss the friction during run-in of the films, and focus only the steady-state behavior.

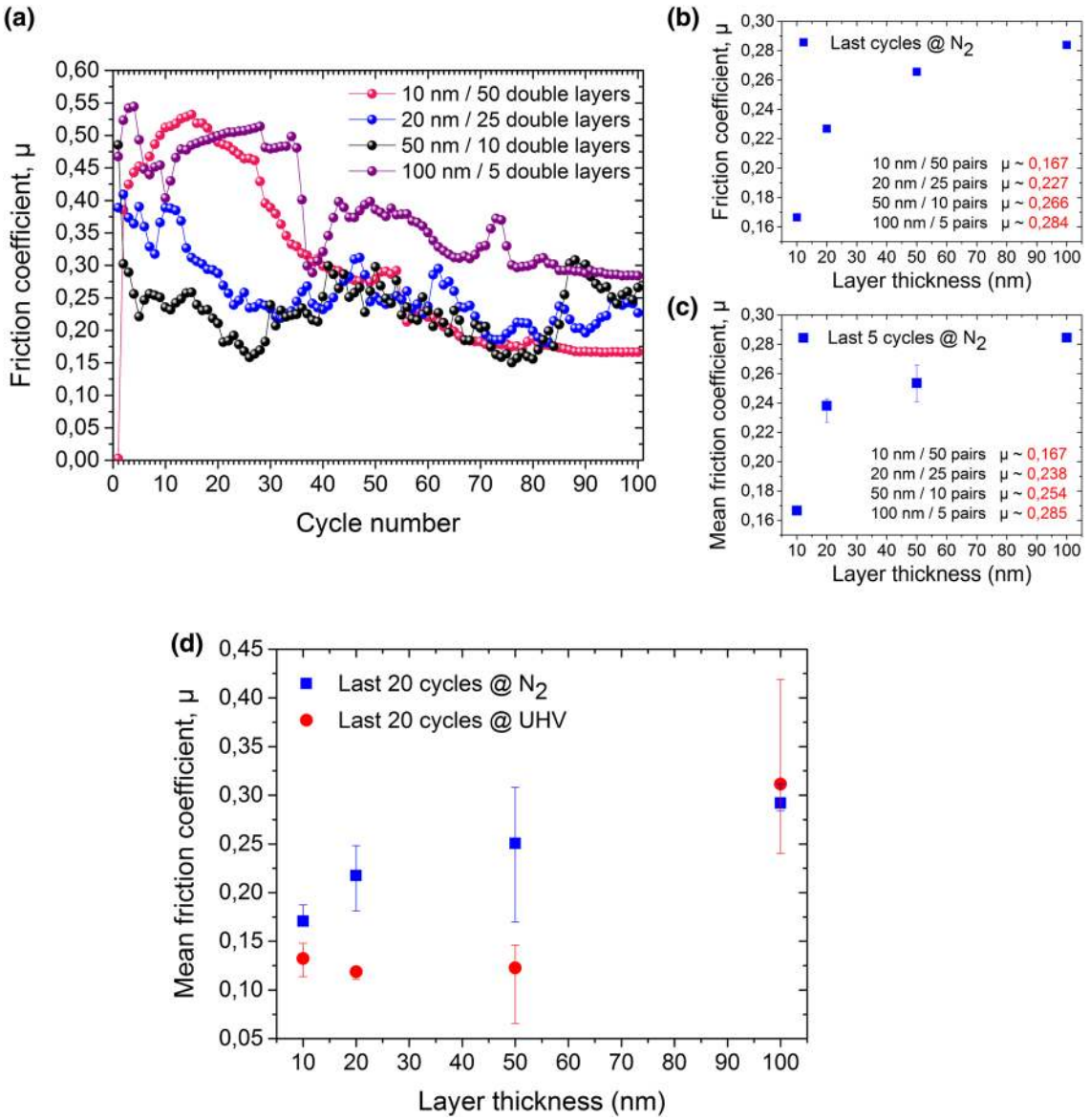

Fig. 2 Frictional behavior of Au–Ni multilayers. **a** Different frictional stability was found throughout sliding for 100 reciprocating cycles. For all tribological systems the friction coefficient drops after the first few cycles. The COF decreases gradually for the systems with 10 or 100 nm layer spacing while for others, the friction decreases suddenly. The 20 and 50 nm layer spacings still showed rather unstable friction behavior towards the end of the experiment, whereas for the other systems stable friction was observed within the last 20 cycles. A significant increase of the COF with increasing layer thickness is clear in the last cycle (**b**) and averaged over the last five cycles (**c**). Error bars in **c** were determined by the fluctuations in friction behavior during sliding as shown in **a**. **d** Comparison of the COF values between UHV conditions and N_2 atmosphere averaged over the last 20 sliding cycles. The COF values for the N_2 atmosphere were larger than that observed under UHV conditions, except the 100 nm sample. Error bars in **d** were determined by the fluctuations in friction behavior during sliding as shown in **a** and in [21]

3.2 Microstructure Evolution of Worn Multilayers

Figure 3a, b presents the cross-sectional micrographs of the 10 nm sample after the friction experiment. In contrast to the previous experiments in UHV, we did not observe any kind of intermixing between Au and Ni layers, as shown in the EDXS maps in Fig. 3c, d. Only the first Au layer was affected, hereafter referred to as the tribolayer (i.e., the region affected by the tribological stress), having around 20 nm thickness separated from the remaining material. The corresponding EDXS maps revealed the existence of Au (Fig. 3c) and the absence of Ni (Fig. 3d) in the tribolayer.

The detailed structural analysis of the 20 nm sample is displayed in Fig. 4. While deformation was confined to the first Au layer, the following Ni layer remained undeformed (Fig. 4a, b). The affected Au layer grew in thickness from

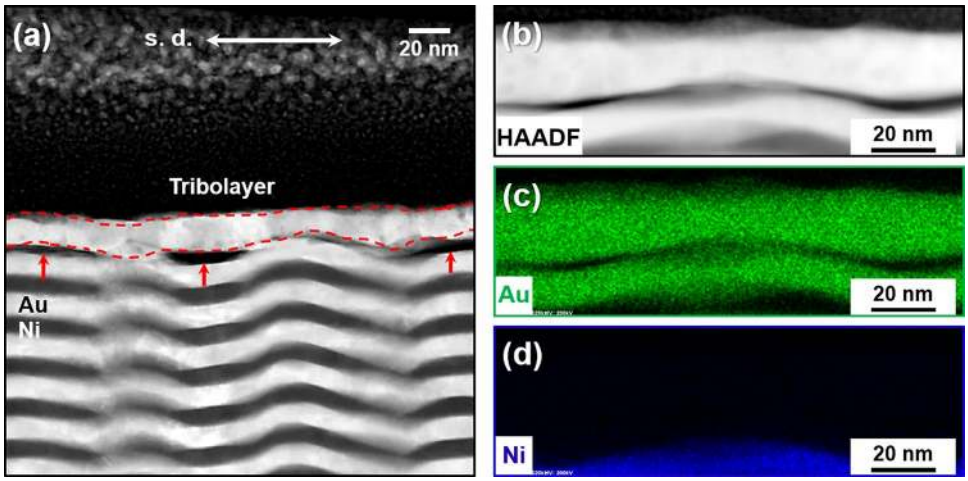

Fig. 3 Characterization of Au–Ni multilayers with 10 nm layer thickness after the friction test in N_2 atmosphere. **a** HAADF STEM cross-section of the worn 10 nm multilayer sample. Detachment of the tribolayer was observed (red arrows). **b** HAADF STEM cross-section of the worn 10 nm multilayer sample. Corresponding EDXS map showing weight concentration of **c** Au and **d** Ni in the tribomaterial. All cross-sections were prepared parallel to the sliding direction (Color figure online)

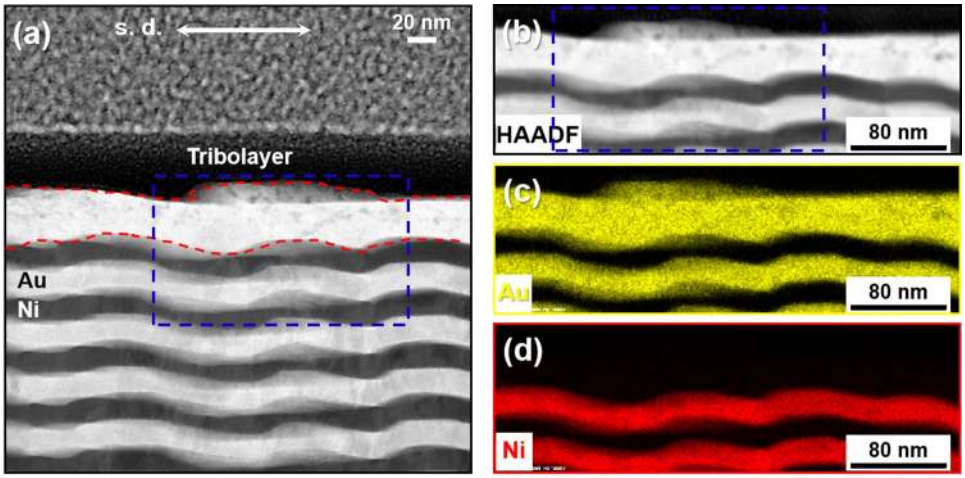

Fig. 4 Characterization of Au–Ni multilayers with 20 nm layer thickness after the friction test in N_2 atmosphere. **a** HAADF STEM cross-section of the worn 20 nm multilayer sample. **b** HAADF STEM cross-section of the worn 20 nm multilayer sample. Corresponding EDXS map showing weight concentration of **c** Au and **d** Ni in the tribomaterial. All cross-sections were prepared parallel to the sliding direction

20 nm to 40–45 nm during shearing, as shown in Fig. 4a. The corresponding EDXS maps revealed the presence of Au (Fig. 4c) and absence of Ni (Fig. 4d) in the tribolayer, again demonstrating the lack of mixing between the multilayers.

For the 50 nm multilayer sample shown in Fig. 5, we observed that the counter body (ruby ball) penetrated the top Au layer and only the bottom portion of the Au remained adhered to the Ni layer below. The cross-sectional STEM image perpendicular to the sliding direction in Fig. 5a depicts the worn portion of the top Au layer with the formation of a void. The HR-TEM image in Fig. 5b also shows the deformation of the uppermost Au layer, where damaged regions are indicated by the yellow arrow.

Figure 6 depicts the worn microstructure of the 100 nm sample subsequent to the friction test under N_2 atmosphere. Comparing to the results of the 50 nm sample, little impact of the tribological stress was observed except for a thinning of the topmost Au layer by 10–30%, as seen in Fig. 6a. Only the first Au layer was plastically deformed while subsequent layers were unaffected. The TEM image in Fig. 6b clearly shows the shear-deformed grains within the tribolayer.

4 Discussion

4.1 Frictional Behavior of Au–Ni Multilayers in Different Environments

As explained in detail in previous work [21], under well-defined UHV conditions the individual layer thickness of the Au–Ni multilayer systems has a strong impact on the resulting friction force. Under UHV, the multilayer samples with the thickness of 10 nm, 20 nm, and 50 nm showed a low COF, while the 100 nm sample resulted in much higher friction under the same sliding conditions. On the other hand, performing the tests in a different environment resulted in different microstructural evolution for each sample except for the 100 nm interlayer spacing. As a result, the friction was different for all cases except for the latter one. Figure 2d shows this difference between the multilayer samples sheared under different environmental conditions. Note that in Fig. 2a, the friction was highly variable as the number of sliding cycles changes

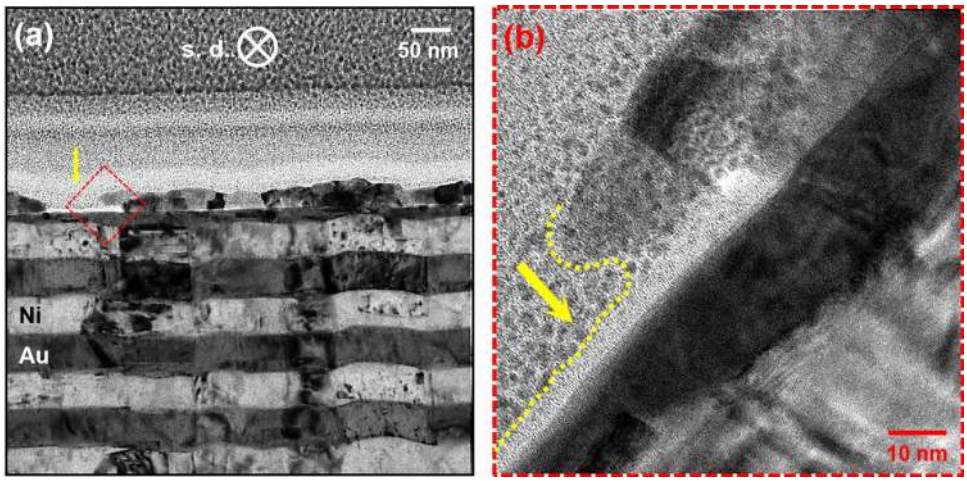

Fig. 5 Characterization of Au–Ni multilayers with 50 nm layer thickness subsequent to the friction test in N_2 atmosphere. **a** BF STEM cross-section of the worn 50 nm multilayer sample. **b** HR-TEM image, marked with the red dashed square in **a**, showing the damaged, crystalline tribolayer. Note that different appearances within the several zones in **b** caused by the mass-thickness contrast. Thicker regions in the tribolayer (and the heavier Au) in the sample appear dark while thinner regions in the tribolayer (and the lighter Ni) in the sample appear with higher contrast. The top Au layer was completely missing in some regions with the formation of voids (yellow arrow in **b**). All cross-sections were prepared perpendicular to the sliding direction

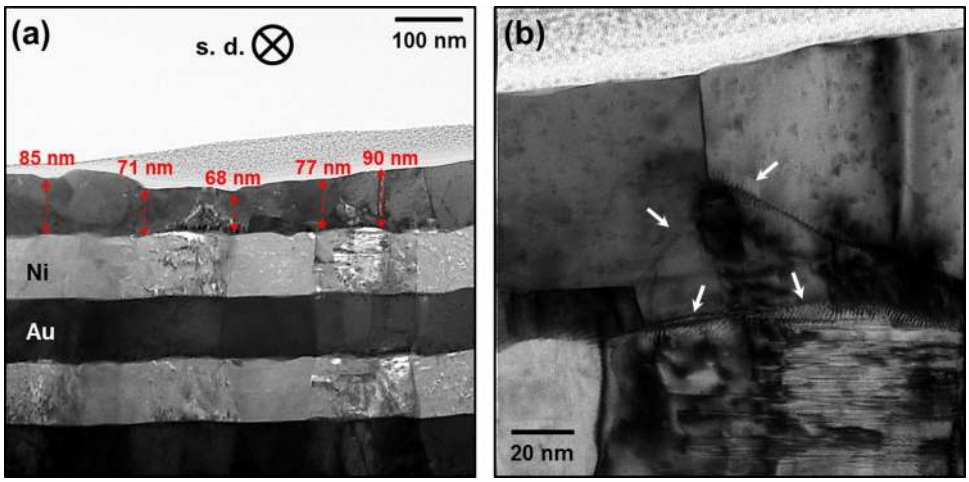

Fig. 6 Characterization of Au–Ni multilayers with 100 nm layer thickness subsequent to the friction test in N_2 atmosphere. **a** BF STEM cross-section of the worn 100 nm multilayer sample. Only the top Au layer was damaged. **b** TEM image showing the shear-induced microstructure in the tribolayer. The white arrows show the accumulation of dislocations at grain boundaries, supporting the conclusion that deformation mechanism is controlled by dislocation motion in this case. All cross-sections were prepared perpendicular to the sliding direction

in N_2 atmosphere, although the COFs at the last cycles were more stable compared to the overall behavior. The final COF values obtained in N_2 atmosphere were larger than those observed under UHV conditions in all cases except for the 100 nm sample. Interestingly, in N_2, where mixing between the Au and Ni is suppressed, the 10 nm, 20 nm, and 50 nm samples show higher friction than in UHV. However there is little difference for the 100 nm sample, where the mixing is not present in either UHV or N_2. Note that the lower friction forces for thinner interlayer spacings under UHV was attributed to the final microstructure resulting from the mechanical mixing of Au and Ni [21]. This mixing is likely linked to the dominant deformation mechanism [24, 25]. As we have already verified the ultrafine grain microstructure in the 10 nm sample via HR-TEM [21], it is likely that grain sizes developed thorough the sliding experiments (due to mechanical mixing) under UHV must be smaller than those in N_2 (except for the 100 nm sample), even though the latter experiments also led to changes in grain size; this is partially the cause of

the fluctuations of the friction data. Because of the smaller overall grain size, lower friction was found under UHV conditions for thinner multilayer samples. Similarly, in N_2, the lowest friction was observed in the 10 nm sample, and this thickness correlates with grains that are close to or smaller than the critical grain size [25].

4.2 Microstructure Evolution of Au–Ni Multilayers in Different Environments

When compared to the microstructural evolution observed under UHV [21], the experiments in nitrogen demonstrate the impact of environment on the resulting microstructure. No mechanical mixing of Au and Ni was observed for the multilayers slid in the nitrogen, in contrast with experiments in UHV. In nitrogen, only the uppermost Au layers were plastically deformed by plowing, and smearing of Au from other regions in the contact was seen for the samples with 10 nm and 20 nm layer thicknesses. As shown in Fig. 4a, for the 20 nm sample shearing has led to an increase in thickness by about a factor of two (thickness after sliding 40–45 nm); this is most probably caused by plowing. A possible explanation for the thickening in this area of the contact can be the accumulation of the material plowed from other areas in contact. For the 10 nm sample, in addition to the thickening of the first Au layer, some parts of the tribolayer (around 15–20 nm) detached from the remainder, leaving a layer < 10 nm (Fig. 3a). This could be the result of higher localized stresses, as plastic deformation can induce the formation and nucleation of cracks beneath the contact, depending on the magnitude of the stress acting on the contacting surfaces [26]. Considering the observation of the 20 nm sample at the position where the FIB lamella was cut, it can be assumed that the detachment of the tribolayer is inhibited in thicker layers. We argue that the roughness of the ruby sphere could have led to different forces in different areas, and the position chosen to monitor the microstructural evolution is of significant importance. FIB cuts prepared parallel to the sliding direction for the 10 nm and 20 nm samples do not reveal the nature of the grooves on the wear track and thus allow us to only observe the plowing behavior throughout sliding. To study this, FIB cuts of the 50 nm and 100 nm samples were prepared perpendicular to the sliding direction, so that the grooves of the wear track can be observed. As seen in Fig. 5 for the 50 nm sample, the same amount of normal stress caused more damage in the top portion of the first Au layer, resulting in the formation of voids in the near-surface material. In contrast, the bottom portion was still adhered to the Ni underlayer. This groove (asperity) on the wear track is one of the more deeply plowed regions, and is likely responsible for local thickening due to the redistribution of the plowed material. Note that this effect is not seen in the other samples. Interestingly, there is overall less damage after sliding of the 100 nm sample due to the larger grain sizes in this system (Fig. 6). The amount of wear is estimated via the thinning of the multilayers.

Figure 7 compares wear tracks from the two different environments. Although similar structures were observed for both tracks, the environments resulted in quite different wear behavior. Much less wear was found for the multilayer samples sheared in N_2 compared to that under UHV, leading to the different amount of deformation. Figure 7a, recorded via AFM, shows a plan view of the wear track for the 20 nm sample sheared under UHV. Lighter colors indicate higher topography whereas darker colors show deeper regions. The side view of the wear track shows that a depth of around 70–80 nm from the surface, in line with the previously discussed microstructural evolution, i.e., mechanical mixing of the Au and Ni [21]. In addition, a pile-up of material ~ 100 nm thick is visible on the surface of the wear track. In contrast, in N_2, there is less wear, as seen from the topographical image of the wear track in Fig. 7b. The side view of this track also reveals the lower wear, with a depth of only 20–25 nm (13 nm in some cases) from the surface, with several localized trenches. This analysis would also corroborate the microstructural evolution of the 20 nm sample sheared in N_2, where no mixing of Au and Ni was observed (see the corresponding EDXS map). Correspondingly, less material pile-up (~ 30 nm) was found on the surface of the wear track.

As stated above and in our previous publication [21], intermixing of Au and Ni layers has been observed in thinner multilayer samples in UHV, including the formation of a shear-induced AuNi alloy phase that does not exist in the binary phase diagram of the Au–Ni system [27]. Modifying the environment, however, led to different microstructural evolution, with no intermixing of Au and Ni layers. X-ray photoelectron spectroscopy (XPS) analysis shown in Fig. 8 reveals that carbon and oxygen are initially present on the topmost surface of the multilayer samples before the friction tests. Note that the multilayer samples were always cleaned via XPS/Ar ion sputtering prior to the friction tests under UHV conditions and the residual adsorbed gases (C and O_2 peaks in the XPS spectrum) were removed. Since the current experiments were carried out under a N_2 atmosphere, there are possible effects of the environment on the sliding contact region. For example, the adsorption of N_2 [28] and NO_2 [29] on Au surfaces has been observed, and the formation of N_2O_3 via the adsorption of NO_2 has been seen on Au (111) [30]. Additionally, the presence of trace hydrocarbons has been shown to be more than sufficient to affect the friction of hard, smooth, and deformation resistant coatings [31]. Hence, the possibility of chemical interactions by hydrocarbons on the uppermost Au layers cannot be excluded in our experimental conditions. It might also be argued that a minute amount of water vapor in the N_2 atmosphere (< 10 ppm O_2 and < 40 ppm H_2O measured) can

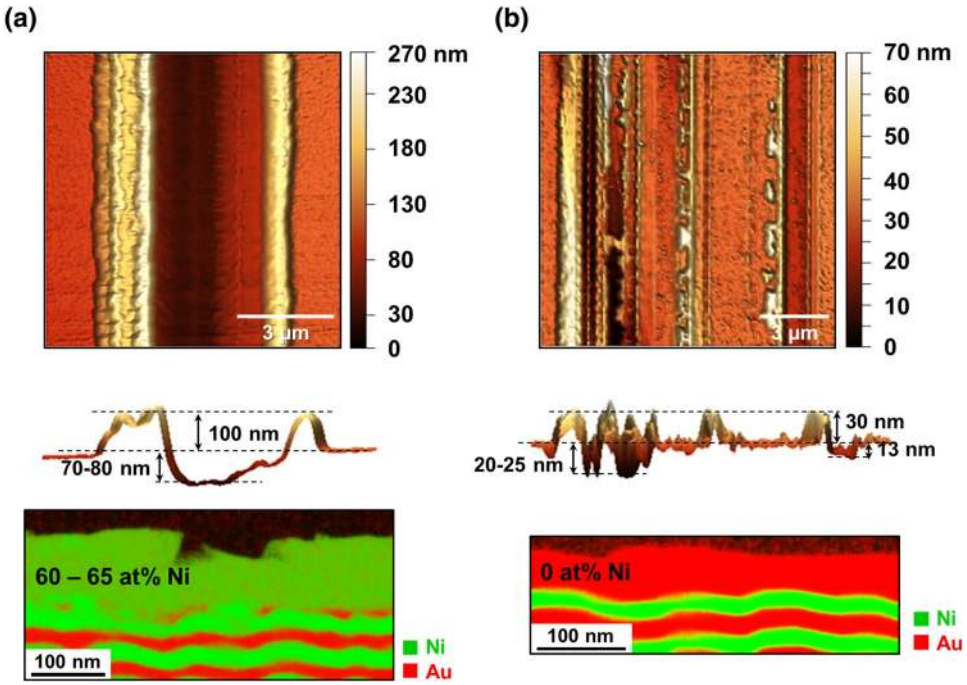

Fig. 7 AFM topography images of the wear tracks for the 20 nm sample after 100 reciprocating cycles of sliding under **a** UHV conditions and **b** N_2 atmosphere showing, from top to bottom, top view, side view of the height, and chemical analysis performed by EDXS. Plowing of the relatively soft multilayers with the hard ruby sphere leads to the creation of grooves in the wear tracks. The side view of the wear track in **a** is in agreement with the microstructure evolution in UHV, where the layers of Au and Ni have mixed. Due to the direct contact between the ruby ball and the multilayer sample at the clean (uncontaminated) interface, the sphere has worn several Au and Ni layers resulting in mixing [21]. The side view of the track in **b** reveals the gentler wear on the sample surface in N_2 environment. The direct contact at the interface is changed by adsorbates, so that only the topmost Au layer is influenced

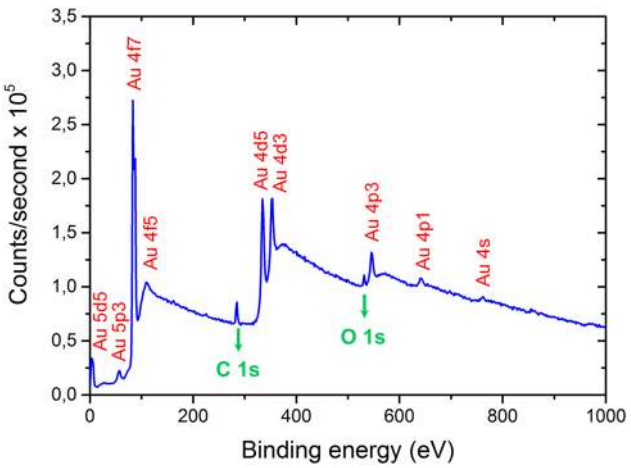

Fig. 8 XPS surface profiles of the Au–Ni multilayer sample. C and O_2 peaks are present on the topmost surface before the friction test

affect the contact between the ruby sphere and the multilayer sample, if the adsorption of water on the initially clean surface of the sapphire [32] is taken into account. Considering this, the presence of water adlayers on the ruby surface could account for the lower wear of the multilayers by causing the shear to occur in the water layer on the ruby sphere. Due to the capillary effects of water, the contact area can increase at the interface, also leading to the observed higher friction in N_2, compared to that in UHV.

In summary, these experiments suggest that adsorption of environmental species, even in a nominally clean N_2 atmosphere; can increase the shear strength (i.e., from capillary forces, in the case of water) between the ruby ball and the multilayer sample. Due to the obvious impact of adsorbates on the apparent shear stresses, the effect of grain size on the friction in the thinner multilayer samples was smaller in dry N_2 than in UHV, even though grain size changed in both conditions. On the other hand, contaminant-free UHV conditions enabled a stronger effect of the grain size on the friction, particularly in thinner multilayer samples, through the formation of a shear-induced AuNi alloy.

5 Conclusion

In this article, friction experiments performed on Au–Ni multilayer samples under dry, ultra-high purity N_2 are reported, and are compared to previous results obtained under UHV [21]. The differences in environment impacted

friction by increasing the COF in N_2, likely due to the absence of grain refinement by mechanical alloying. The COFs of each multilayer system in N_2 were larger than under UHV, except for the 100 nm samples. Much lower wear was found for the multilayers sheared in N_2, resulting in different amounts of deformation. No mixing was observed between the Au and Ni layers for thinner multilayer samples under N_2, in contrast with UHV. Despite the environment being nominally inert, the role of trace hydrocarbons can have a remarkable impact on friction behavior when the rubbing surfaces are wear resistant and smooth [31]. While we found deformation of the uppermost Au layers from plowing of material throughout sliding, material transfer from other areas in the contact was also occasionally observed, leading to thickening of the tribolayer. The sublayers appeared unaffected for all samples. For the 10 nm sample only, detachment of the tribolayer was found.

Acknowledgements Open Access funding provided by Projekt DEAL. The authors gratefully acknowledge support from the Deutsche Forschungsgemeinschaft through the Heisenberg Programme (DI 1494/4-1 and DI 1494/5-1). Harald Leiste, Michael Stüber, and Sven Ulrich are gratefully acknowledged for their contribution to the growth of Au–Ni multilayer samples and XRD characterization. The authors also thank Dominic Linsler and Eberhard Nold for the nanoindentation measurements and XPS analysis. This work was accomplished as part of the Research Travel Grant provided by the Karlsruhe House of Young Scientists (KHYS) of KIT. The authors also acknowledge the Sandia National Laboratories Laboratory Directed Research and Development (LDRD) program for funding this work. This work was performed, in part, at the Center for Integrated Nanotechnologies, an Office of Science User Facility operated for the U.S. Department of Energy (DOE) Office of Science. Sandia National Laboratories is a multi-mission laboratory managed and operated by National Technology and Engineering Solutions of Sandia, LLC., a wholly owned subsidiary of Honeywell International, Inc., for the U.S. Department of Energy's National Nuclear Security Administration under contract DE-NA-0003525. The views expressed in the article do not necessarily represent the views of the U.S. DOE or the United States Government.

References

1. Roberts, E.W.: Space tribology: its role in spacecraft mechanisms. J. Phys. D **45**, 503001 (2012)
2. Gola, A.: Deformation of metallic multilayers: an atomistic study of the relationship between structure and deformation mechanisms. Karlsruhe (2019)
3. Godet, M.: The third body approach: a mechanical view of wear. Wear **100**, 437–452 (1984)
4. Bowden, F.P., Tabor, D.: Mechanism of metallic friction. Nature **150**, 197–199 (1942)
5. Lancaster, J.K.: A review of the influence of environmental humidity and water on friction, lubrication and wear. Tribol. Int. **23**(6), 371–389 (1990)
6. Grillo, S.E., Field, J.E.: The friction of CVD diamond at high Hertzian stresses: the effect of load, environment and sliding velocity. J. Phys. D **33**, 595–602 (2000)
7. Kim, H.I., Lince, J.R., Eryilmaz, O.L., Erdemir, A.: Environmental effects on the friction of hydrogenated DLC films. Tribol. Lett. **21**(1), 51–56 (2006)
8. Li, H., Xu, T., Wang, C., Chen, J., Zhou, H., Liu, H.: Tribochemical effects on the friction and wear behaviors of a-C: H and a-C films in different environment. Tribol. Int. **40**(1), 132–138 (2007)
9. Dudder, G.J., Zhao, X., Krick, B., Sawyer, W.G., Perry, S.S.: Environmental effects on the tribology and microstructure of MoS_2–Sb_2O_3–C films. Tribol. Lett. **42**(2), 203–213 (2011)
10. Stoyanov, P., Stemmer, P., Järvi, T.T., Merz, R., et al.: Friction and wear mechanisms of tungsten–carbon systems: a comparison of dry and lubricated conditions. ACS Appl. Mater. Interfaces **5**, 6123–6135 (2013)
11. Cui, L., Lu, Z., Wang, L.: Environmental effect on the load-dependent friction behavior of a diamond-like carbon film. Tribol Int. **82**, 195–199 (2015)
12. Marchetto, D., Feser, T., Dienwiebel, M.: Microscale study of frictional properties of graphene in ultra high vacuum. Friction **3**(2), 161–169 (2015)
13. Stempflé, P., Stebut, J.: Nano-mechanical behaviour of the 3rd body generated in dry friction—feedback effect of the 3rd body and influence of the surrounding environment on the tribology of graphite. Wear **260**(6), 601–614 (2006)
14. Mougin, K., Gnecco, E., Rao, A., Cuberes, M.T., Jayaraman, S., McFarland, E.W., Haidara, H., Meyer, E.: Manipulation of gold nanoparticles: influence of surface chemistry, temperature, and environment (vacuum versus ambient atmosphere). Langmuir **24**(4), 1577–1581 (2008)
15. Greiner, C., Felts, J.R., Dai, Z., King, D.P., Carpick, R.W.: Controlling nanoscale friction through the competition between capillary adsorption and thermally activated sliding. ACS Nano **6**(5), 4305–4313 (2012)
16. Egberts, P., Ye, Z., Liu, X.Z., Dong, Y., Martini, A., Carpick, R.W.: Environmental dependence of atomic-scale friction at graphite surface steps. Phys. Rev. B **88**, 035409 (2013)
17. Chen, X., Han, Z., Li, X., Lu, K.: Lowering coefficient of friction in Cu alloys with stable gradient nanostructures. Sci. Adv. **2**, 1601942 (2016)
18. Hutchings, I., Shipway, P.: Tribology: Friction and Wear of Engineering Materials. Elsevier, Cambridge (2017)
19. Buckley, D.H.: Surface Effects in Adhesion, Friction Wear and Lubrication. Tribology, vol. 5. Elsevier, Amsterdam (1981)
20. Tabor, D.: Junction growth in metallic friction: the role of combined stresses and surface contamination. Proc. R. Soc. Lond. Ser. A **251**, 378–393 (1959)
21. Cihan, E., Störmer, H., Leiste, H., Stüber, M., Dienwiebel, M.: Low friction of metallic multilayers by formation of a shear-induced alloy. Sci. Rep. **9**(9480), 1–10 (2019)
22. Giannuzzi, L.A., Stevie, F.A.: A review of focused ion beam milling techniques for TEM specimen preparation. Micron **30**(3), 197–204 (1999)

23. Zeng, G., Tan, C.K., Tansu, N., Krick, B.A.: Ultralow wear of gallium nitride. Appl. Phys. Lett. **109**(5), 1–6 (2016)
24. Yamakov, V., Wolf, D., Phillpot, S.R., Mukherjee, A.K., Gleiter, H.: Deformation-mechanism map for nanocrystalline metals by molecular-dynamics simulation. Nat. Mater. **3**, 43–47 (2004)
25. Argibay, N., Chandross, M., Cheng, S., Michael, J.R.: Linking microstructural evolution and macro-scale friction behavior in metals. J. Mater. Sci. **52**, 2780–2799 (2017)
26. Suh, N.P.: Update on the delamination theory of wear. In: Rigney, D.A. (ed.) Fundamentals of Friction and Wear of Materials, pp. 43–71. ASM, Pittsburgh (1981)
27. Raynor, G.V.: The alloying behaviour of gold. Gold Bull.: J. Gold Sci. Technol. Appl. **9**(1), 12–19 (1976)
28. Krim, J., Dash, J.G., Suzanne, J.: Triple-point wetting of light molecular gases on Au (111) surfaces. Phys. Rev. Lett. **52**, 640–643 (1984)
29. Wickham, D.T., Banse, B.A., Koel, B.E.: Adsorption of nitrogen dioxide on polycrystalline gold. Catal. Lett. **6**, 163–172 (1990)
30. Bartram, M.E., Koel, B.E.: The molecular adsorption of NO_2 and the formation of N_2O_3 on Au (111). Surf. Sci. **213**, 137–156 (1989)
31. Argibay, N., Babuska, T.F., Curry, J.F., Dugger, M.T., Lu, P., Adams, D.P., et al.: In-situ tribochemical formation of self-lubricating diamond-like carbon films. Carbon **138**, 61–68 (2018)
32. Schildbach, M.A., Hamza, A.V.: Clean and water-covered sapphire (1102) surfaces: structure and laser-induced desorption. Surf. Sci. **282**, 306–322 (1993)